Stratonovich Waves Driven by Space-Time Gaussian Noise: Second Moment and Exact Asymptotics

Le Chen

Version 1.0.0, November 16, 2026

Abstract

This reading edition explains how fast the second moment grows and what determines its limiting constant. We follow the argument from construction of the solution to an independent upper bound at the correct time scale, and then to identification of the constant. The spatial covariance is a nonnegative positive-definite homogeneous Radon measure in dimensions one, two or three. The temporal covariance is a fractional power. The limiting constant is a supremum over all nonnegative smooth compact spacetime controls, with the original covariance amplitude and gradient coefficient one. The Gaussian cost is half the variance of the associated Gaussian functional. We give the definitions, main statements and connecting deductions, with links to the full proofs in the book. The book also contains the finite-order calculations and alternative estimates.

Working-draft status. This short account accompanies version 1.0.0 of the book, which contains the full proofs. Linking its statements to the book does not mean that the whole argument has been accepted; an independent check of the mathematics is still open.

Contents

1 From a guitar in a sandstorm to moment asymptotics **3**

2 Model, constant and main results **3**
2.1 The original model 3
2.2 The full positive-control domain 4
2.3 The two main statements 5
2.4 Two interpretations and their tradeoffs 7

3 One canonical solution and all mixed terms **9**
3.1 Ordered chains and fixed orders 9
3.2 Why the order of limits matters 11

4 The independent upper estimate **11**
4.1 Finite interval models 11
4.2 Positive terminal coefficients and temporal domination 13
4.3 From prelimit bounds to the same canonical moment 13

5 The wave solution path and source convergence **14**
5.1 The phase and its two variances 14
5.2 The source has to retain the original noise 15

6 A lower bound with one Gaussian cost **16**
6.1 Fixed controls and a global change of law 16
6.2 Source first, then the large-time estimate 17
6.3 Dilation, positivity and independent finiteness 18

7 Physical mean operators and uniform spectral estimates **18**
7.1 The spatial extension that the proof needs 18
7.2 Scalar time compactness and the mean 19

8 Gaussian estimates for the point upper bound **20**
8.1 The radius and the one Gaussian quadratic cost 20
8.2 Uniform products and a signed variational expression 21
8.3 Averages of squares, not a rough point trace 21

9 Identifying the limiting constant **22**
9.1 Singular Gram matrices are allowed 22
9.2 Bounds for the optimizing controls 24
9.3 The cutoff limit and the final deduction 24

10 Calibrations and useful consequences **25**
10.1 Finite orders and comparisons 25
10.2 Spatial white noise: an energy and bounds, not an exact evaluation . . . 26

11 Where the detailed proofs are supplied **26**

1 From a guitar in a sandstorm to moment asymptotics

Imagine a guitar left outside during a sandstorm. Grains strike a string at unpredictable places and times, and the string carries each disturbance away. Walsh used this picture in his 1984 Saint-Flour lectures, published in 1986 [17, p. 282, (1.14)]. His worked example idealizes the string as infinite, initially at rest, and driven by additive white noise. The integral formulation makes sense of motion too irregular for the classical derivatives in the wave equation. Forty years since that landmark exposition, the questions extend from constructing the motion to measuring its growth.



Figure 1: AI illustration by Le Chen, SPDE-Visuals. CC0 (public domain). Not a simulation.

Dalang's integration theory [13] widened the treatment of singular Green kernels and spatial covariance. Probabilistic moment methods [14] and explicit one-dimensional second-moment formulas [5] brought the long-time fluctuations into focus. Exact asymptotics for static Skorohod noise [2] and static Stratonovich noise [11] then sharpened the question: what is the leading constant, and how does the meaning of the noise product affect it?

The present paper asks this question for the second moment with fractional temporal correlation and Stratonovich multiplication. We give an upper bound at the correct scale and a variational expression for the second-moment limit. The working-draft notice records the review status. This account follows selected developments since Walsh's lectures; it does not cover the earlier history or all later work. The book's account in *Technical Notes*, Section 1.1, p. 1 and its literature comparison retain the hypotheses and distinctions behind these milestones.

2 Model, constant and main results

2.1 The original model

We use the Stratonovich interpretation of

$$\partial_t^2 u = \Delta u + \dot{W} u, \qquad u(0,x) = 1, \qquad \partial_t u(0,x) = 0. \tag{2.1}$$

The noise is centered Gaussian. Write $a = \alpha_0$ for its temporal exponent. Its covariance, understood on real smooth compact tests, is $|s-t|^{-a}\Gamma(x-y)$. We retain the amplitude in Γ.

Hypothesis 2.1 (Original covariance)**.** Let $d \in \{1,2,3\}$, $0 < a < 1$, and $\alpha + a < 2$. Either $0 < \alpha < d$, or $\alpha = d = 1$. The spatial covariance Γ is a nonnegative, even,

positive-definite tempered Radon measure with positive even tempered spectral measure μ, in the distributional convention

$$\Gamma = \int_{\mathbb{R}^d} e^{i\xi\cdot x}\mu(\,\mathrm{d}\xi), \qquad \Gamma(cA) = c^{d-\alpha}\Gamma(A) \quad (c > 0).$$

The zero measure is allowed. No radial density, angular density, product factorization or finite total spectral mass is assumed.

This is precisely the model class of *Technical Notes*, Hypothesis 1.2.1, p. 3. In particular, it includes one-dimensional spatial white noise and singular nonradial measures in higher dimensions. The positive wave Green measure G_t is supported on the closed ball of radius t and has mass t, in each of the three dimensions. At zero frequency its Fourier multiplier is t, the continuous value of $\sin(t|\xi|)/|\xi|$.

Set

$$k = 3 - \alpha, \qquad q = 4 - \alpha = k + 1, \qquad \kappa = \frac{4 - \alpha - a}{3 - \alpha}. \tag{2.2}$$

Here $k > 1$. The construction in Section 3 fixes the canonical solution of (2.1); all limits below refer to this same solution.

2.2 The full positive-control domain

Let $I = (0, 1)$. The covariance Hilbert space H_I is the completion of real $C_c^\infty(I \times \mathbb{R}^d)$ modulo its covariance null space, with

$$\langle \Phi, \Psi \rangle_{H_I} = \int_{I^2} |s - t|^{-a} \int_{\mathbb{R}^d} \Gamma(\,\mathrm{d}y) \int_{\mathbb{R}^d} \Phi(s, x)\Psi(t, x - y)\,\mathrm{d}x\,\mathrm{d}s\,\mathrm{d}t. \tag{2.3}$$

Thus, W is isonormal on this space. The integral convention, rather than an implicit Fourier factor, fixes the action used below. Define

$$\mathcal{C}_{\mathrm{pos}} = \{\Psi \in C_c^\infty(I \times \mathbb{R}^d; \mathbb{R}) : \Psi \geq 0,\ \Psi \neq 0\}. \tag{2.4}$$

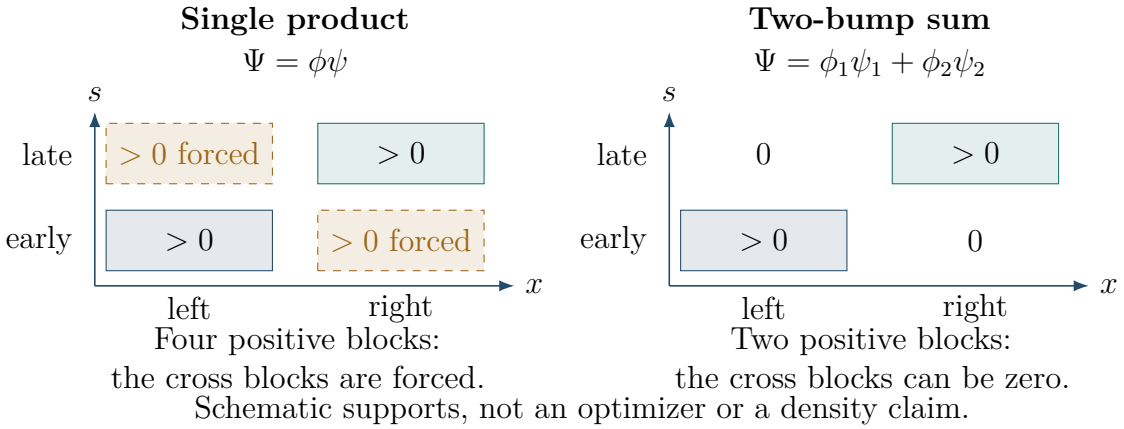


Figure 2: The full control class allows spatial profiles to change with time, as in this sum of two smooth nonnegative product bumps that no single time–space product can represent. The full class is infinite-dimensional; see *Technical Notes*, Theorem 11.2.6, p. 281.

This includes functions that do not factor into one temporal function and one spatial function. It is a class in a separable covariance space; no nonseparable topological space is required. For $\Psi \in \mathcal{C}_{\mathrm{pos}}$, put

$$h_{\Psi,s}(x) = \int_I |s-t|^{-a}(\Gamma * \Psi_t)(x)\,\mathrm{d}t, \tag{2.5}$$

$$v_\Psi = \|[\Psi]\|_{H_I}^2 = \int_{I\times\mathbb{R}^d} \Psi(s,x)h_{\Psi,s}(x)\,\mathrm{d}x\,\mathrm{d}s, \tag{2.6}$$

$$\lambda_{\Psi,s}^2 = \sup_{\substack{f\in H^1(\mathbb{R}^d;\mathbb{R})\\ \|f\|_2=1}} \left\{\int_{\mathbb{R}^d} h_{\Psi,s}f^2 - \|\nabla f\|_2^2\right\}, \tag{2.7}$$

$$I_\Psi = \int_0^1 \lambda_{\Psi,s}\,\mathrm{d}s, \qquad S_c^{\mathrm{pos}} = \sup_{\Psi\in\mathcal{C}_{\mathrm{pos}}}\{cI_\Psi - v_\Psi/2\}, \quad c>0. \tag{2.8}$$

For nonzero covariance, $h_{\Psi,s}$ is globally bounded, smooth and nonnegative, and its time dependence is Lipschitz in the uniform norm. The operator $-\Delta - h_{\Psi,s}$ is self-adjoint on H^2, with form domain H^1. Its bottom is uniformly negative on $[0,1]$; hence the square root in (2.7) is positive and I_Ψ is finite. These are the conclusions of *Technical Notes*, Lemmas 7.3.1, p. 189 and 7.3.2, p. 189, followed by *Technical Notes*, Proposition 7.3.3, p. 190. They do not require an eigenfunction at the unmasked spectral bottom. For $\Gamma = 0$, all these means, variances, rates and variational expressions are zero.

2.3 The two main statements

The independent estimate uses the exact resolvent mass

$$R_\alpha = \frac{\alpha\pi\mu(B_1)}{2\sin(\pi\alpha/2)}. \tag{2.9}$$

Its finiteness follows from homogeneity and $0<\alpha<2$.

Theorem 2.2 (Independent upper bound)**.** *Under Hypothesis 2.1, there is a finite constant $C(\alpha,a)$, depending only on these two exponents, such that for $T\ge 1$ and every fixed x,*

$$\mathbb{E}|u_\Gamma(T,x)|^2 \le e(T+2)^d \exp\left\{C(\alpha,a)R_\alpha^{1/(3-\alpha)}T^\kappa\right\}. \tag{2.10}$$

For zero covariance $u=1$, and the estimate is direct.

This is *Technical Notes*, Theorem 3.3.8, p. 88. Its proof uses no finiteness assumption on the variational expressions in (2.8). We give its argument before using it to prove that those variational expressions are finite.

Theorem 2.3 (The second-moment constant)**.** *Under Hypothesis 2.1, for every fixed x,*

$$\lim_{T\to\infty} T^{-\kappa}\log\mathbb{E}|u_\Gamma(T,x)|^2 = C_2(\Gamma,a) = S_2^{\mathrm{pos}} = 2^{q/k}S_1^{\mathrm{pos}}. \tag{2.11}$$

The domain, covariance norm and rates in this formula are exactly (2.3)–(2.8). The kinetic coefficient is one and the action is $v_\Psi/2$. For nonzero covariance $0<C_2(\Gamma,a)<\infty$. For zero covariance $C_2=0$.

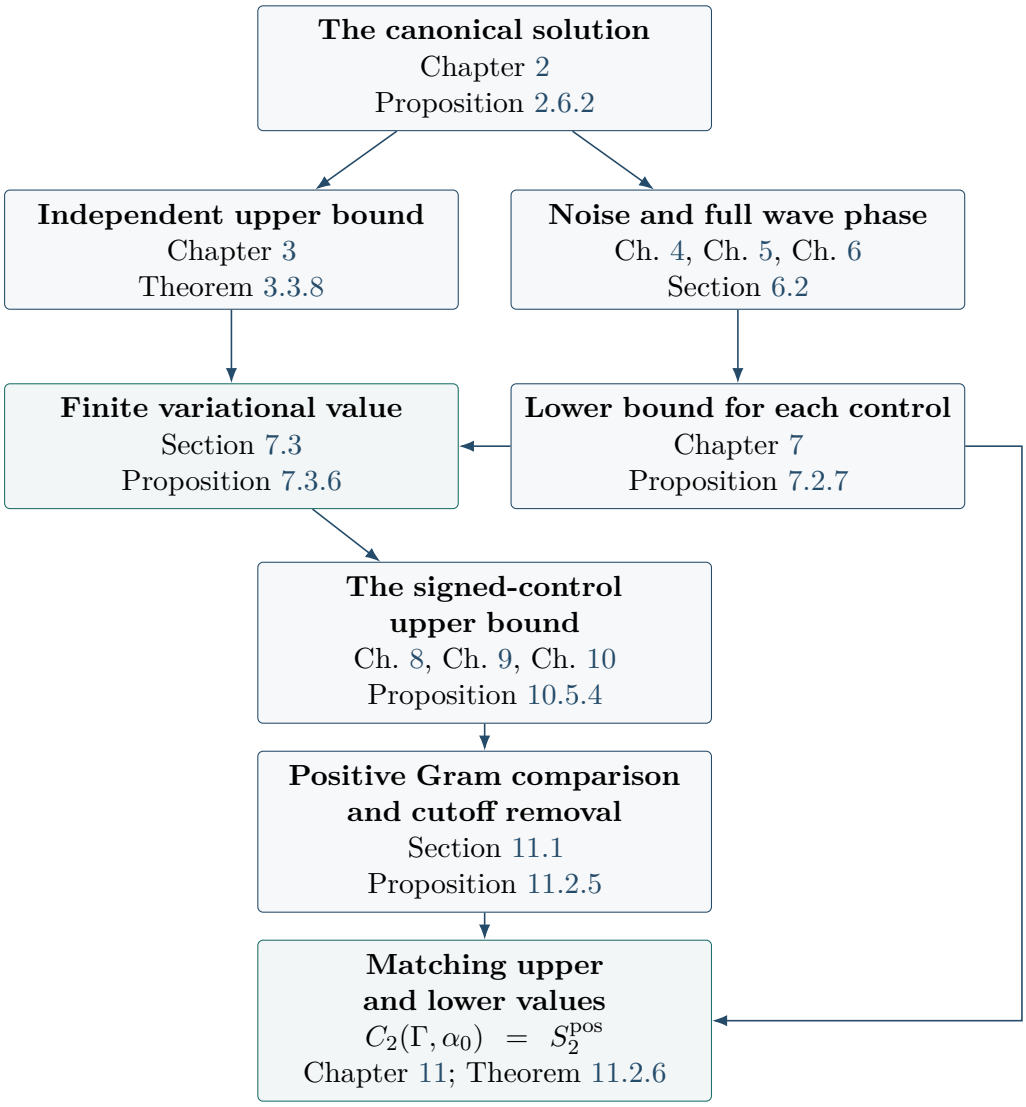


Figure 3: The principal proof dependencies, with links to chapters and results in the technical companion. The independent upper bound and the fixed-control lower bound first give a finite variational lower value. Further operator and Gaussian estimates give a signed-control upper bound for the same point moment. Positive Gram comparison and cutoff removal identify the two values. Arrows show principal uses; each box also has the hypotheses and earlier inputs stated at its linked destination. They do not assert independence of successive time blocks. The zero-covariance case is included in the final theorem.

Theorem 2.3 is the statement of *Technical Notes*, Theorem 11.2.6, p. 281. The symbol S_1^{pos} is an auxiliary variational expression. The formula does not identify it with the first-moment limit of the solution or with Chen's printed variational constants. The author version of Chen's paper proves two-sided first-moment bounds; its earlier arXiv version is not used to replace them by an exact limit [9].

2.4 Two interpretations and their tradeoffs

The noise product is part of the equation. Skorohod integration uses the Malliavin divergence and Wick products. For the linear equation with deterministic data, orthogonal Wiener chaoses make second moments a sum of squared chaos norms, and the mean is the free wave. For adapted white-in-time integrands this agrees with Itô integration. With correlated time noise, Skorohod integration does not provide a martingale structure.

Stratonovich iteration uses ordinary products of regularized noise. It retains self-pairings and unequal iteration-order cross terms; these change the mean and complicate second moments. One can still regroup trace terms into orthogonal Wiener chaoses [1]. Its appeal is the connection to wave evolution in smooth random potentials, provided the chosen approximation converges. Its cost is controlling those contractions and, for singular noise, proving convergence or specifying counterterms. There is no universal wave conversion formula between the two interpretations. Neither one supplies a general wave maximum principle. Model choice comes before comparison of methods or constants.

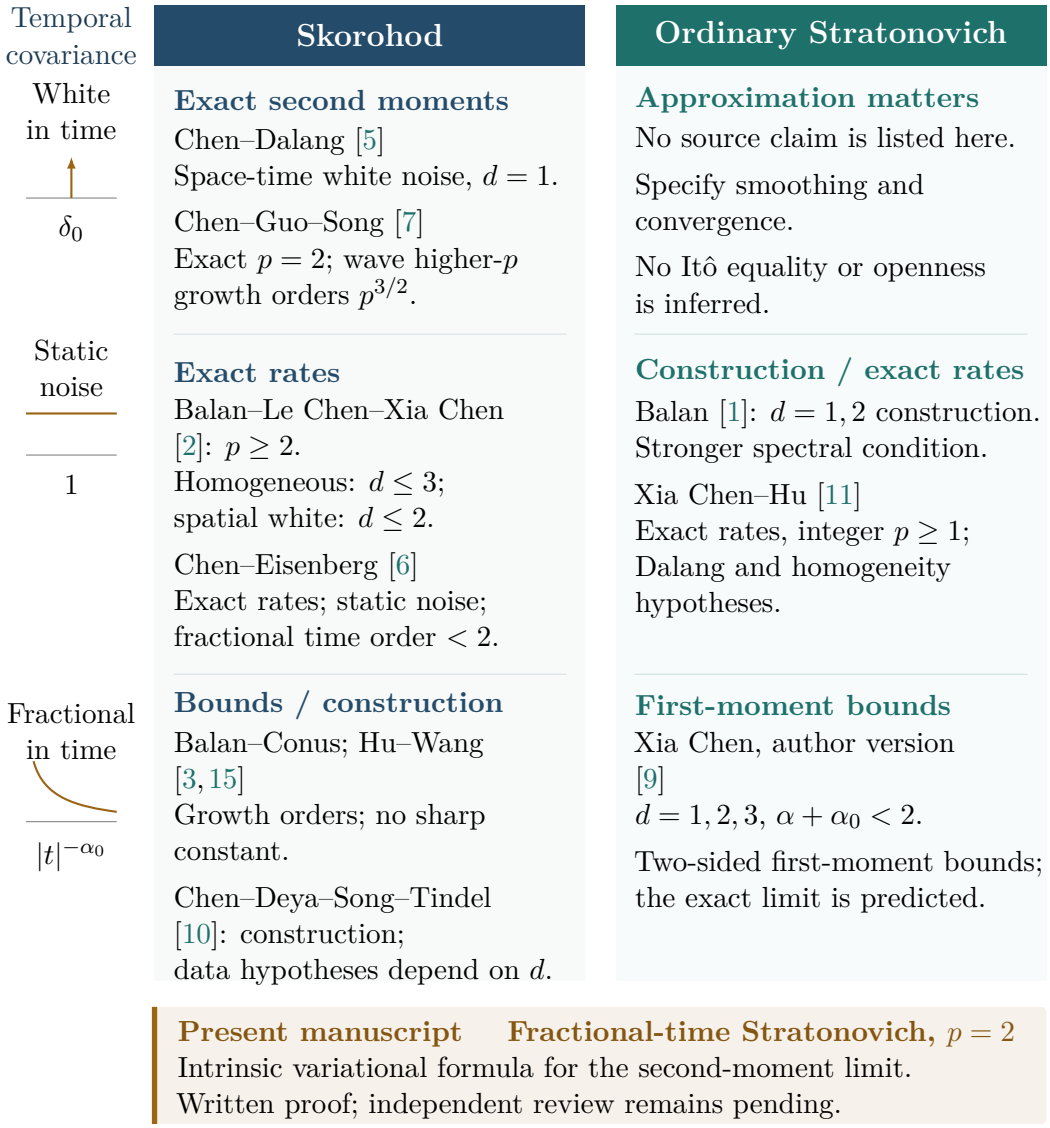


Figure 4: A reading map of selected results, not an implication diagram. The rows distinguish temporal covariance models. The small sketches show covariances, not noise paths or limits between rows. Every source retains its spatial covariance, dimension and initial-data hypotheses; the technical literature review gives the detailed comparison. Exact second moments and matching higher-moment growth orders are different conclusions. Fractional differentiation in Chen–Eisenberg is not fractional temporal noise. The highlighted band records the present written claim; independent review remains pending. The white-in-time Stratonovich cell is not an assertion that the problem is open or that it equals the Itô model.

Which results are comparable? Chen–Dalang [5] obtain explicit white-noise wave second moments. Chen–Guo–Song [7] also obtain matching $p^{3/2}$ wave moment-growth orders, with nonoptimal higher-moment constants. Balan–Song [4] distinguish an upper

second Lyapunov exponent for general covariances from an actual limit in their Riesz case. For static Skorohod noise, Balan–Le Chen–Xia Chen [2] prove exact asymptotics; Chen–Eisenberg [6] treat a related family with fractional differential time order strictly below two. Fractional time differentiation is distinct from fractional temporal noise. For the latter, Balan–Conus [3] and Hu–Wang [15] give growth-order comparisons under their respective hypotheses. On the static Stratonovich side, Balan [1] constructs solutions and Xia Chen–Hu [11] establish homogeneous moment asymptotics, subject to the normalization qualifications in the technical notes.

The present written proofs identify the second-moment limit and an intrinsic constant for temporally correlated Stratonovich noise, retaining self-pairings and the original covariance class. They do not identify a numerical closed constant or sharp all-moment asymptotics. Independent review status is separate from these manuscript claims. The fuller comparison in *Technical Notes*, Section 1.3, p. 7 distinguishes construction, growth-order and exact-limit results, including their dimensions, covariance and data restrictions. Separate ongoing projects with Raluca Balan and Jinxin Wang concern colored Skorohod noise in dimensions one and two, and white-in-time noise in dimensions one through three. No unpublished result from those projects is used here.

Remark 2.4 (How to use the proof package)**.** This reader gives the complete definitions, the principal intermediate statements and the deductions connecting them. The supplied *Technical Notes* give the detailed proofs of the cited intermediate results, as well as the retained alternative estimates and calibrations. A reference marked "Technical Notes" gives that document's theorem number and printed page and links to its statement. The reader alone does not replace those detailed proofs. The complete package consists of both documents.

3 One canonical solution and all mixed terms

3.1 Ordered chains and fixed orders

Let g_n be the ordered n-vertex wave kernel with data $(1, 0)$, including its terminal Green factor, and set $I_0 = 1$. For positive noise widths, each regularized term is an ordinary Gaussian polynomial. Its products contain all Wick pairings, including self-pairings within either chain. If the chain lengths are m, n, the expectation vanishes when $m + n$ is odd. When $m + n$ is even, it is the sum over all pair partitions of the combined $m + n$ vertices. There is no orthogonality rule that removes the terms $m \neq n$. Time reversal can identify moments at a fixed terminal time; it is not a pathwise equality with a forward integral on the same noise.

Lemma 3.1 (Construction and summation)**.** *At every fixed pair of orders, remove the inner Green regularization first at fixed positive external noise widths. The resulting terms have a joint L^2 limit as all external widths tend to zero at arbitrary relative rates, on the original Gaussian probability space. Denote these limits by $I_n = S_n(g_n)$. For each finite T, there are constants θ_0, C, independent of all the widths, such that the vertexwise*

terms are bounded by

$$q_n(T) = e^{\theta_0 T}\frac{C^{n/2}T^n}{\sqrt{n!}}, \qquad \sum_{n\geq 0}\sqrt{n+1}\,q_n(T) < \infty.$$

Consequently, $u = \sum_{n\geq 0} I_n$ *in* L^2*, locally uniformly in the stated moment bounds, and*

$$\mathbb{E}|u(T,x)|^2 = \sum_{m,n\geq 0}\mathbb{E}[I_m(T,x)I_n(T,x)]. \tag{3.1}$$

This is the canonical solution obtained from the same regularized classical equations. Its physical mild equation is identified under the corresponding ordinary Gaussian multiplication and summation bounds.

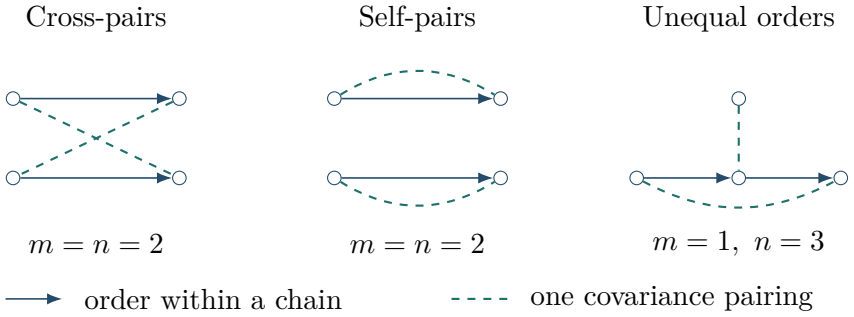


Figure 5: Three permitted pairing contributions. Each chain has its own time order; no common interleaving is imposed by the picture. Stratonovich products include self-pairs and unequal orders, as well as cross-pairs. These examples do not list every pairing. See *Technical Notes*, Proposition 2.1.1, p. 31.

The fixed-order part is *Technical Notes*, Lemmas 2.5.1, p. 44 and 2.5.2, p. 46. The summable vertex bound is *Technical Notes*, Lemma 2.6.1, p. 50; the full mixed identity and physical identification are *Technical Notes*, Propositions 2.1.1, p. 31 and 2.6.2, p. 52. No uniqueness assertion is needed or made. These are separate assertions: a formula for fixed-order moments alone does not identify a full physical mild solution.

The finite two-chain product envelope used here is proved in *Technical Notes*, Lemma 2.4.1, p. 40. It bounds each pairing integral by a finite maximum of admissible products of the three norms. The maximizing assignment may depend on the kernels and edge data; no single assignment for every kernel family is asserted. Chen's universal bound is retained as source context [9, Theorem 3.1]. The application uses the damped wave norms and the independent-origin translated-covariance Cauchy–Schwarz bridge in *Technical Notes*, Lemmas 2.3.1, p. 33 and 2.3.2, p. 36. The first norm has the absolute value *around the inner* Fourier–Laplace integral. For the heat-smoothed damped wave this inner integral is nonnegative:

$$\int_0^\infty \int_{\mathbb{R}^d} e^{-\lambda t + i\xi\cdot x}e^{-\vartheta t}(p_\eta * G_t)(x)\,\mathrm{d}x\,\mathrm{d}t = \frac{e^{-\eta|\xi|^2/2}}{(\vartheta+\lambda)^2+|\xi|^2}.$$

Independent time origins and independent spatial variables are retained in the second norm. These estimates supply the norm inputs to the self-contained product envelope, with its hypotheses checked before the all-order argument.

3.2 Why the order of limits matters

For fixed external width, the random factor in an ordinary Green convolution is fixed while its inner Green width tends to zero. If $F(z)$ is this $L^2(\Omega)$-valued factor and $\tau = t-s$, then Bochner Fubini gives

$$\int (p_\eta * G_\tau)(\,\mathrm{d}z)F(z) = \int G_\tau(\,\mathrm{d}z) \int p_\eta(w)F(z+w)\,\mathrm{d}w.$$

At fixed external noise widths, use the spatially uniform bound $\sup_z \|F(z)\|_2 \le M$, uniformly over $0 \le s \le T$. Stationarity, the vertex estimates and finite-degree Gaussian multiplication supply this finite M; it may depend on these widths. Only the modulus $\omega(r)$ is local, on a fixed neighborhood of the Green support. For $0 < r < 1$ the difference from $\int G_\tau(\,\mathrm{d}z)F(z)$ is bounded by

$$\tau\{\omega(r) + 2M \Pr(|Z_\eta| > r)\}, \qquad Z_\eta \sim N(0, \eta I_d). \tag{3.2}$$

At fixed r, the Gaussian tail tends to zero; then $r \downarrow 0$. The bound $2\tau M$ permits time integration. Multiplication on the finite Gaussian polynomial spaces used here supplies M at this fixed external width. It is not an assertion that multiplication by an unbounded Gaussian is bounded on arbitrary $L^2(\Omega)$.

Proof of the summation assertion in Lemma 3.1. Cauchy–Schwarz gives $|\mathbb{E}I_m I_n| \le q_m(T)q_n(T)$. The double series of these bounds is finite. Finite partial sums converge in L^2, so their squared norms converge; absolute double summability identifies the limit with (3.1). The same bound permits the required sum–expectation interchanges. Formula (3.2) explains the inner Green passage; the joint fixed-order limit and the summable tail then remove the external widths and the order cutoff. The detailed vertex and multiplication estimates are the cited Technical Notes lemmas. This proves the mixed-summation assertion of Lemma 3.1. □

4 The independent upper estimate

4.1 Finite interval models

The estimate starts with finitely many temporal covariance intervals, Gaussian modes and spatial frequency and box cutoffs. Finite Gaussian modes alone do not make Gaussian multiplication bounded. For each selected word, truncate the Hermite degree of color i at $N_i \ge r_i$, where r_i counts its insertions. Starting from the constant polynomial 1 (the Gaussian vacuum), every prefix of that word stays below its degree cutoff, including creation followed by annihilation. The compressed and uncompressed selected words are

therefore identical. This is not an identity between full propagators at a fixed Hermite cutoff. These degree and spatial cutoffs give bounded operators for the numerical-range argument. The Gaussian modes produced by earlier factors are retained; scalar solution-value moments on successive intervals are not multiplied. The phase is a displacement–velocity pair. Its complex operator is not generally self-adjoint; the numerical-range estimate is applied through the four ordered roots used in *Technical Notes*, Lemma 3.2.1, p. 61. The bounded theorem of Crouzeix–Palencia, with universal constant $1+\sqrt{2}$, applies to a bounded operator on a complex Hilbert space and functions holomorphic on a neighborhood of its closed numerical range [12, author preprint v1, Theorem 6, pp. 5–6, and (3), p. 1]. At fixed selected word and positive noise widths, the Gaussian-mode and frequency cutoffs are then removed by strong convergence. The full flow is constructed separately by summing its coefficients; it is not identified with one fixed-degree truncated flow.

The Gaussian contraction used here follows directly from the nonnegative positive-definite covariance and homogeneity. Uniformly in positive spatial smoothing and finite mode and frequency cutoffs,

$$\sum_m \|(\rho^2-\Delta)^{-1/2} M_{e_m} f\|_2^2 \le R_\alpha \rho^{\alpha-2} \|f\|_2^2.$$

Here e_m are the spatial coefficient functions of one smoothed isonormal field. This is the dimension-independent input of *Technical Notes*, Lemma 3.3.1, p. 71. No later Gaussian Rayleigh estimate or static asymptotic coefficient is a premise of this interval argument.

Lemma 4.1 (Finite-model bound and physical identification)**.** *Sort the lengths of the intervals decreasingly and suppose $h_i \le LT/i$ and $\sigma_i^2 \le c h_i^{-a}$. For real Schwartz data $v=(f,g)$ use $\|v\|_\rho^2 = \|f\|_2^2 + \|(\rho^2-\Delta)^{-1/2} g\|_2^2$. If $\mathcal{U}(T;s)$ is the phase flow with common scalar amplitude s, then, for $j \ge 1$,*

$$\left| [s^{2j}] \mathbb{E} \|\mathcal{U}(T;s)v\|_{1/T}^2 \right| \le \frac{C^j R_\alpha^j T^{(4-\alpha-a)j}}{(j!)^{3-\alpha}} \|v\|_{1/T}^2. \tag{4.1}$$

Here $C = C(\alpha, a, L, c)$ is independent of the finite interval family, Gaussian modes, frequency cutoff and spatial noise width. The family from three shifted interval grids has fixed admissible values of L, c. Summing gives the exponential scale T^κ.

The finite interval model has a bound with parameter-only exponential constant and spatial dependence through R_α. In its derivation, occupied Gaussian colors are handled jointly, and a fresh Gaussian vacuum is introduced only where its stated comparison is valid. The selected-word estimates retain row and column, creation and annihilation, and both phase entries. The comparison with the full time-integration cube has coefficient one and introduces no extra factorial. Remove frequency and box cutoffs before invoking positivity of the physical Green diagrams. At fixed finite family of time intervals and positive noise widths, the resulting polynomial and flow are the interval-field Gaussian objects, for both displacement and velocity.

This is *Technical Notes*, Proposition 3.3.5, p. 82. The full finite Fock deductions are in Technical Notes, Sections 3.2–3.3, including *Technical Notes*, Lemma 3.3.2, p. 72.

The separate variance estimate in Technical Notes, Section 3.1, controls both the Born term and the second-order mean term. It is a first-variance tool, not a substitute for the all-order coefficient estimate (4.1). Neither term can be dropped from that variance calculation. No covariance order for arbitrary phases is used.

4.2 Positive terminal coefficients and temporal domination

For the smooth positive Green model, the terminal Wick coefficients are nonnegative. The terminal $2n$-simplex has volume $T^{2n}/(2n)!$. At fixed positive widths this yields an entire series and the physical identification in *Technical Notes*, Lemma 3.3.6, p. 85. A bound depending on the maximum of that fixed smooth covariance proves this identification; it is not the uniform upper bound.

The singular temporal kernel is dominated numerically by a positive three-grid interval kernel. Choose $6T \le H_0 < 12T$ and lengths $h_\ell = H_0 2^{-\ell}$, $\ell \ge 0$. Grid j has endpoints $h_\ell(n + (-1)^\ell(j-1)/3)$, $n \in \mathbb{Z}$. Let $\mathcal{D}_j$ contain its intervals meeting $[0, T]$. Put

$$K_\infty(s,r) = 6^a \sum_{j=1}^{3} \sum_{J \in \mathcal{D}_j} |J|^{-a} 1_J(s) 1_J(r), \qquad K_N \uparrow K_\infty. \tag{4.2}$$

Keeping levels through N defines K_N. The sorted interval lengths obey $h_i \le 78T/i$ and the weights have $\sigma_i^2 = 6^a h_i^{-a}$. Thus, $L = 78$ and $c = 6^a$ apply in (4.1). For a source cutoff $\eta > 0$, put $\gamma_\eta^0 = K_\eta$, where K_η is the temporal Laplace prefix in Section 5.2. The comparison is

$$\gamma_\eta^0(s-r) \le |s-r|^{-a} \le K_\infty(s,r).$$

It does *not* assert $\gamma_\eta^0 \le K_N$ for arbitrary finite N. For each finite positive diagram, compare with K_∞ and then use positive monotone convergence of K_N. These interval covariances need not be stationary. The comparison is made at the physical positions before any use of original-noise time reversal. It is a comparison of numbers in positive diagrams, not convergence of the interval fields to the original noise and not an operator order on phase covariances.

4.3 From prelimit bounds to the same canonical moment

Localization uses a compact datum equal to one on the backward cone. Its position component and locality give the factor $e(T+2)^d$. There is no hidden bound by derivatives of that datum growing exponentially with T. The uniform positive prelimit bound, at coupling $r > 1$, has the form

$$B(T; r) = e(T+2)^d \exp\left\{C(\alpha, a)(r^2 R_\alpha)^{1/k} T^\kappa\right\}. \tag{4.3}$$

The spectral amplitude has already been included once in R_α; it is not multiplied into the covariance a second time.

Proof of Theorem 2.2 from the finite-model inputs. First fix the physical order and positive external noise widths. Lemma 4.1 removes the finite spatial cutoffs and identifies

the interval model. Positivity and (4.2) pass its bound through the increasing finite collections of time intervals. The terminal Wick series then gives the full positive prelimit bound (4.3).

To remove noise widths, fix an order cutoff and use the joint square and cross limits of Lemma 3.1. The enlarged-coupling estimate, for example with $r = 2$, gives a uniform geometric tail for the original-coupling series. This is the role of *Technical Notes*, Lemma 3.3.7, p. 87. Let the widths tend to zero at this fixed cutoff, then send the cutoff to infinity. The estimate at $r = 1$ gives (2.10). The separate identification with the physical mild solution in *Technical Notes*, Proposition 2.6.2, p. 52 says that this canonical series is the solution of (2.1); it does not enter the numerical prelimit estimate. At $\Gamma = 0$ every positive-order term is zero and $u = 1$. This proves Theorem 2.2. □

5 The wave solution path and source convergence

5.1 The phase and its two variances

Use the energy phase $E = H^{1/2} \times H^{-1/2}$ and its extension $F = E \oplus \mathbb{R}^2$. An element (e, c_1, c_2) represents the total initial distributions $(e_1 + c_1, e_2 + c_2)$. Constants are not in E. The free evolution on F is

$$S_F(t)(e, c_1, c_2) = (S_E(t)e, c_1 + tc_2, c_2). \tag{5.1}$$

Thus, the free constant displacement and velocity columns are both retained. A constant potential's first displacement response is $\lambda t^2/2$; the first response to constant initial velocity is $\lambda t^3/6$. This distinguishes the two columns even at the lowest perturbative order.

Choose fixed exponents

$$\begin{gathered} 0 < \gamma < \min\{1/2, (2-\alpha)/2\}, \\ 1/2 < \theta < \beta < \min\{1 - a/2, (3 - a - \alpha)/2\}. \end{gathered} \tag{5.2}$$

The strict threshold makes the choices possible. The spatial covariance rows, their Sobolev adjoints and the normalized time-kernel norm squared give both variances $\sum A_j A_j^*$ and $\sum A_j^* A_j$. They require different balanced Sobolev substitutions. The original spectral measure μ may be singular. The even auxiliary mask measure ν_R has a continuous density and uniform translated-ball growth, as in *Technical Notes*, Proposition 4.1.2, p. 95. The estimates use that growth; they require no uniform density bound. The reflected measure in the adjoint calculation and the continuous zero-frequency wave quotient are part of the calculation, not additional assumptions. These computations are *Technical Notes*, Propositions 4.2.1, p. 102, 4.2.5, p. 108 and 4.2.6, p. 110.

Lemma 5.1 (Same-noise compact path and full phase flow)**.** *For each fixed physical mask, the integrated noise has a centered Gaussian version in a closed separable subspace of $C^\theta([0,T]; \mathcal{K}(E))$, on the original probability space. Its finite noise projections converge there in every finite L^p. At all times the operators are compact on one common event. Its*

norm has a Gaussian square-exponential bound. The extension to F retains both constant columns. For the corresponding correlated smooth sources, Young flows converge in every finite moment in the uniform operator norm on F, with the stated Gaussian uniform integrability. At each positive source width the flow is the ordinary physical wave flow; its tested averages agree with the canonical moment construction.

The path is *Technical Notes*, Proposition 5.1.1, p. 126. Its compact-tail argument first uses a common pair of positive compact variance envelopes and eigenvalue domination to prove trace decay. Finite Gaussian compressions retain both variances. This produces interval Schatten moment tails; the subsequent path limit is in the operator norm, not a claim of a C^θ Schatten-valued path. A moving rank-one projection without a common compact envelope would not justify that step. The extension and flow statements are *Technical Notes*, Propositions 6.2.2, p. 155, 6.2.4, p. 157 and 6.2.5, p. 158, with *Technical Notes*, Lemma 6.2.6, p. 160 and *Technical Notes*, Proposition 6.2.7, p. 161 for physical identification.

5.2 The source has to retain the original noise

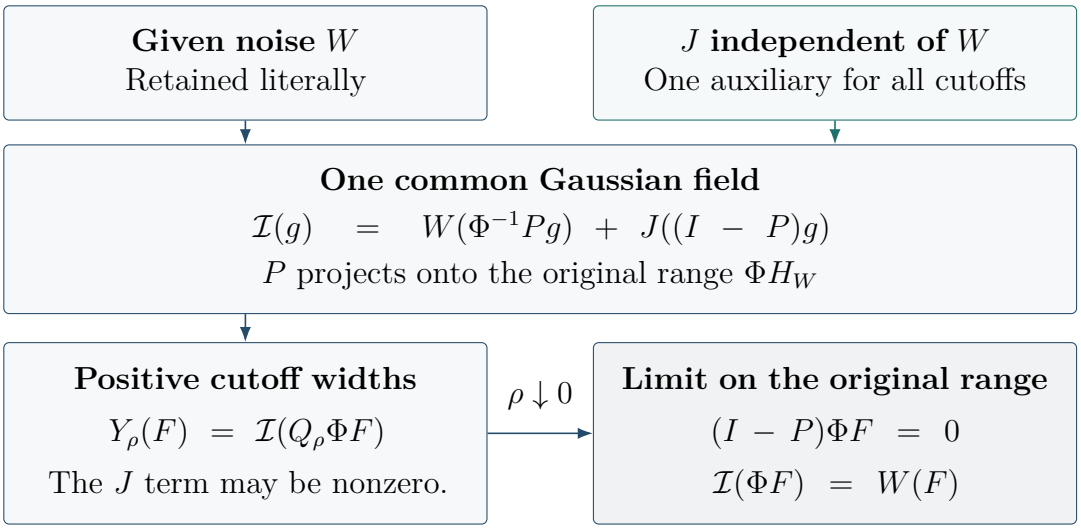
Use one product extension retaining the original W literally. The feature isonormal family $\mathcal{I}$ satisfies $\mathcal{I}(\Phi h) = W(h)$; one fixed auxiliary isonormal family J completes the orthogonal complement. Spatial heat smoothing and a temporal Laplace prefix act as commuting contractions in feature space. The positive-cutoff sources may use J and need not be measurable with respect to W alone. Their limit of the integrated noise operator and the canonical observables are measurable with respect to the original W. This is *Technical Notes*, Lemma 5.2.4, p. 141.

For positive widths $\rho = (\varepsilon, \eta)$, the exact joint law is

$$\operatorname{Cov}(Y_{\varepsilon,\eta}(t,x), Y_{\varepsilon',\eta'}(s,y)) = K_{\max(\eta,\eta')}(t-s)(p_{\varepsilon+\varepsilon'} * \Gamma)(x-y),$$

where $K_\eta(v) = \Gamma_E(a)^{-1} \int_0^{\eta^{-1}} e^{-\lambda|v|}\lambda^{a-1}\,\mathrm{d}\lambda$ and Γ_E is Euler's Gamma function. Thus, the temporal operation is a Laplace prefix, not convolution; spatial widths add and temporal widths take their maximum. The finite Gaussian comparison, the two compact variance tails and the path limit give convergence at fixed mask and time horizon; see *Technical Notes*, Proposition 5.2.5, p. 143. Ordinary Picard identities and Bochner-tested averages give the physical interpretation. For a compact deterministic shifted potential, the primitive is constructed separately. Its support may extend outside the mask; the union is still compact. The shifted source bound contains the sum of the deterministic primitive norm and the integrated-noise path norm.

For an operator path of Hölder exponent $\theta > 1/2$, the linear Young integral on a sufficiently short interval is a contraction. Its local length is chosen from the full norm of the integrated operator path. Concatenation gives a growth bound with a power below two in that Gaussian norm. This is why the resulting Gaussian moments and source uniform integrability are available. The phase extension and both columns are used in these bounds; a solution-value estimate alone would not permit composition at successive times.



The limit retains the original random variable $W(F)$.

Figure 6: One coupling for every cutoff. The sources may depend on the auxiliary noise J, but the limiting noise and operator path retain the given W. A new independent copy is not chosen at each cutoff. Here P projects onto ΦH_W; it is not a time cutoff. See *Technical Notes*, Lemma 5.2.4, p. 141 and *Technical Notes*, Proposition 5.2.5, p. 143.

6 A lower bound with one Gaussian cost

6.1 Fixed controls and a global change of law

Fix $\Psi \in \mathcal{C}_{\mathrm{pos}}$ and initially fix a physical mask. The associated smooth positive mean has a uniformly negative spectral bottom, obtained from a common compact trial after a sufficiently large fixed radius is chosen. Positive ground profiles for this compact family support the cone estimate. An unmasked ground eigenfunction is not assumed. The two-component cone is stable under the wave flow.

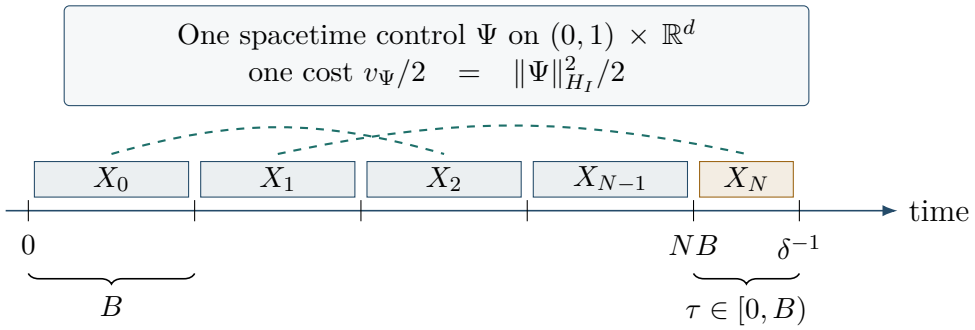
In the fast formulation, put $\delta = T^{-\kappa}$ and $r_T = T\delta$. Exact covariance scaling identifies the law of $u(Tt, r_T x)$ with the canonical solution V_δ of

$$\delta^2 \partial_t^2 V_\delta = \Delta V_\delta + \sqrt{\delta}\, \dot{W} V_\delta, \qquad (V_\delta, \partial_t V_\delta)|_{t=0} = (1, 0).$$

This is a law identity, not a pathwise uniqueness assertion. The fast blocks retain the given original Gaussian family. The relevant Gaussian change of law has one scalar $Z = W(\Psi)$, with variance v_Ψ. For the complete norm-Borel block tuple X, its deterministic mean shift H satisfies

$$\mathbb{E} j(X) = \mathbb{E}\left[e^{-Z/\sqrt{\delta} - v_\Psi/(2\delta)} j(X + H)\right] \tag{6.1}$$

for every nonnegative norm-Borel j, including extended integrals. This is *Technical Notes*, Proposition 7.2.2, p. 177. There is one Gaussian quadratic cost. Disjoint time intervals are not treated as independent covariance Hilbert spaces.



Correlated blocks; ordered evolution carries $(u, \partial_t u)$.
The last block may be empty. Example: $N = 4$.

Figure 7: The true partition in fast time. Here $N = \lfloor 1/(\delta B) \rfloor$ and $\tau = \delta^{-1} - NB$. All blocks come from the same noise and a single control on the whole time interval. The change-of-law density has cost $v_\Psi/(2\delta)$; the displayed $v_\Psi/2$ is its normalized cost. The proof does not multiply independent block probabilities or add separate Gaussian costs. See *Technical Notes*, Lemma 7.2.1, p. 176 and *Technical Notes*, Proposition 10.2.4, p. 246.

The moment bound for each block and a union bound, with an even moment order chosen above the stated threshold, make the maximum block error small with probability tending to one. On the same event impose $|Z| \le \varepsilon/\sqrt{\delta}$. The latter event also has probability tending to one. The density in (6.1) then costs at most $(v_\Psi/2 + \varepsilon)/\delta$ in the logarithm. The positive cone multiplies the deterministic exponential gains through both displacement and velocity; it does not multiply scalar random moments. Rebasing and the final, possibly shorter time interval are handled by *Technical Notes*, Lemma 7.2.5, p. 182.

6.2 Source first, then the large-time estimate

Before changing law or taking $\delta \downarrow 0$, keep δ and the finite block partition fixed and remove the regularized source products in L^2 under the original measure. The full F flow convergence, moment bounds for products and the ordinary physical cone identities give this passage. Only after it is justified is (6.1) applied to the norm-Borel limiting functional. No tilted-measure source limit is silently substituted for this step. The scaling identity in law then identifies the original point moment. The resulting lower estimate, followed by removal of the fixed physical mask, is

$$\liminf_{T\to\infty} T^{-\kappa} \log \mathbb{E}|u_\Gamma(T,x)|^2 \ge 2I_\Psi - v_\Psi/2 \qquad (\Psi \in \mathcal{C}_{\mathrm{pos}}). \tag{6.2}$$

Its detailed statements are *Technical Notes*, Propositions 7.2.6, p. 183, 7.2.7, p. 186 and 7.3.4, p. 191. The same original stationarity extends the point estimate to each fixed x. Removing the mask here is a deterministic Rayleigh approximation; the stochastic noise is not ordered by a mask.

6.3 Dilation, positivity and independent finiteness

For $r > 0$ define

$$(D_r\Psi)(s,x) = r^{d+2-\alpha}\Psi(s,rx). \tag{6.3}$$

The physical Radon change of variables and the unitary change in the Rayleigh test give

$$h_{D_r\Psi,s}(x) = r^2 h_{\Psi,s}(rx), \qquad v_{D_r\Psi} = r^q v_\Psi, \qquad I_{D_r\Psi} = rI_\Psi. \tag{6.4}$$

For example, the Radon pushforward contributes $r^{\alpha-d}$; it differs from the Lebesgue Jacobian. These are *Technical Notes*, Lemma 7.3.5, p. 193.

Proposition 6.1 (The positive variational expression is finite and homogeneous)**.** *For nonzero covariance,* $0 < S_c^{\mathrm{pos}} < \infty$ *and* $S_c^{\mathrm{pos}} = c^{q/k} S_1^{\mathrm{pos}}$ *for every* $c > 0$.

Proof. For $r_c = c^{1/k}$, equations (6.4) give

$$cI_{D_{r_c}\Psi} - v_{D_{r_c}\Psi}/2 = c^{q/k}(I_\Psi - v_\Psi/2).$$

Dilation is a bijection of the full class $\mathcal{C}_{\mathrm{pos}}$, proving the scaling identity. For one fixed test with $I_\Psi, v_\Psi > 0$, sufficiently small r makes $rI_\Psi - r^q v_\Psi/2 > 0$. Equation (6.2) bounds every variational expression with $c = 2$ by the same point liminf. The independent upper estimate (2.10) bounds its limsup by a finite number. Thus, $S_2^{\mathrm{pos}} < \infty$, and scaling gives finiteness for every c. This is exactly the order of the argument in *Technical Notes*, Proposition 7.3.6, p. 193. This proves Proposition 6.1. □

7 Physical mean operators and uniform spectral estimates

7.1 The spatial extension that the proof needs

A smooth physical covariance pairing is not automatically a bounded map on the completed phase space. The intervening argument is important even when the covariance has no density. The deterministic Fourier bound in *Technical Notes*, Lemma 8.2.3, p. 200 makes the smooth spatial ratio finite without a stochastic moment estimate. The temporal equilibrium profile supplies smooth positive spacetime controls for the separate score inequality in *Technical Notes*, Proposition 8.2.4, p. 201. Polarization and density then give the four-linear H^1 estimate of *Technical Notes*, Proposition 8.2.5, p. 202. The fractional product estimate *Technical Notes*, Lemma 8.3.1, p. 207 uses this physical extension to reach the $H^{1/2}$ and $H^{-1/2}$ phase indices. Thus, the logical order is the smooth ratio, the four-linear extension, then the fractional products. Skipping the middle extension would leave the completed mean operators without their required domain.

For singular measures the underlying pairing is

$$B_\Gamma(f,h) = \int_{\mathbb{R}^d}\int_{\mathbb{R}^d} f(x)h(x-y)\,\mathrm{d}x\,\Gamma(\,\mathrm{d}y).$$

Tonelli in x shows that Lebesgue-null representatives at either position do not change this integral. The full H^1 extension therefore uses function classes, not a pointwise restriction to a singular support chosen arbitrarily. The formal threshold remains the original $\alpha + a < 2$.

7.2 Scalar time compactness and the mean

On $L^2(I)$ let K have kernel $|s-t|^{-a}$. For the temporal covariance space H_t, its canonical isometry $\iota : H_t \to L^2(I)$ identifies the temporal mean as

$$C_t = K^{1/2}\iota : H_t \longrightarrow L^r(I), \qquad 2 < r < 2/a.$$

This map is compact. It is not Hilbert–Schmidt into L^2. Compactness of C_t does not imply compactness of $C_t \otimes I$ on an infinite-dimensional spatial factor. The required compactness at fixed physical radius comes from the spatial mean map as well; see *Technical Notes*, Propositions 8.3.4, p. 209 and 8.3.5, p. 210.

Fix a real even root profile $0 \le \eta \le 1$, smooth compact, equal to one on B_1 and supported in $\overline{B}_2$. Set $m_R(x) = \eta(x/R)^2$, $R \ge 1$. The mask occurs once in the potential. The radius-uniform construction on E is

$$\mathcal{T}_R = T_R(C_t \otimes I_{H_{\mathrm{sp}}}), \qquad \|\mathcal{T}_R\|_{H_I \to L^r(I;\mathcal{K}(E))} \le C_{\mathrm{mean}} = M_0\|C_t\|. \tag{7.1}$$

Here H_{sp} is the original spatial covariance completion. For a smooth test the operator is $\mathcal{T}_R\Phi(s)(u,v) = (0, m_R h_{\Phi,s} u)$. This extends to every $\Phi \in H_I$ by completion. The constant M_0 is independent of R. The complete row, tails and extension are *Technical Notes*, Proposition 9.1.4, p. 221. At zero covariance the spatial covariance Hilbert space H_{sp} and joint covariance space H_I are zero, and these spatial and full mean maps vanish. The pure temporal space H_t and its kernel K remain unchanged.

Choose the auxiliary exponents so that

$$\nu = 1/\theta < 2, \qquad (1-\theta)^{-1} < r < 2/a, \tag{7.2}$$

with θ as in (5.2). For a completed multiplier $L(u,v) = (0, Vu)$ let $k_L = \|L\|$. The unique real supported distribution V is identified by testing against one compact function equal to one on the mask support. Its lift to F is used only for physical identification; its lift constant may depend on R and enters no uniform estimate.

Lemma 7.1 (Uniform energy spectral rate)**.** *On the completed mean class, the form $q_V(f) = \|\nabla f\|_2^2 - \langle Vf, f\rangle$ is closed on H^1. Its self-adjoint operator H_V has bottom $\beta(V) \le 0$. Put $\lambda(L) = \sqrt{-\beta(V)}$. For $K \ge \max(1, k_L)$ and $t \ge 0$,*

$$-K^2 \le \beta(V) \le 0, \qquad \|P_V^E(t)\| \le 8(1+K)^2(1+t)e^{\lambda(L)t}, \tag{7.3}$$

$$|\lambda(L_V) - \lambda(L_W)| \le \sqrt{(K+2)\|L_V - L_W\|} \tag{7.4}$$

when both norms are at most K. Every displayed constant uses the E norm, not a radius-dependent F lift norm.

This is *Technical Notes*, Proposition 10.3.2, p. 251. The form construction uses [16, Theorem 2.14 and Theorem 3.6] with its hypotheses checked for the original form. Ordered resolvents give the square-root form comparisons. With $c = 2 + K^2$ they give $D((H_V + c)^{1/4}) = H^{1/2}$, with dual scale $H^{-1/2}$. The graph-domain argument supplies the required $H^{3/2}$ inclusion; it does not assert $D(H_V) = H^2$ for a rough completed potential. Unit test functions translated away from the potential, with kinetic energy tending to zero, give $\beta(V) \leq 0$.

For the true slow-cell average $\mathcal{A}_\delta$, scalar compactness gives

$$\omega_\delta = \|(\mathcal{A}_\delta - I)C_t\|_{H_t \to L^r} \longrightarrow 0$$

at fixed coarse block length. The operator field then satisfies, uniformly in R and $\|\Phi\| \leq M$,

$$\|\mathcal{A}_\delta \mathcal{T}_R \Phi - \mathcal{T}_R \Phi\|_{L^r} \leq M_0 M \omega_\delta, \qquad \mathrm{Rate}_R(\Phi) = \int_I \lambda(\mathcal{T}_R \Phi(s))\, \mathrm{d}s. \tag{7.5}$$

The rate averages converge uniformly on the whole covariance Hilbert ball, by *Technical Notes*, Proposition 10.3.3, p. 254 and (7.4). This is an estimate for the mean field. It does not replace that field by the scalar temporal map alone.

8 Gaussian estimates for the point upper bound

8.1 The radius and the one Gaussian quadratic cost

The spatial localization radius is $R_\delta = \delta^{-1} + 2$. The radius estimates construct common compact envelopes after the specified spatial rescalings, and bound the moments of the integrated operators on each block. At each fixed δ, hence fixed finite R_δ, remove the source widths and projection cutoffs first. Only then send $\delta \downarrow 0$, using the quantitative moments for a fixed admissible even Q, with radius factor $R^{d/Q}$. The expected-norm estimate contains $\delta^{(1-a)/2} R_\delta^{d/Q} \leq 3^{d/Q} \delta^{(1-a)/2 - d/Q} \to 0$ in that strict Q window. This is not uniform-in-R source convergence or an unguarded diagonal choice of source widths and radius. These are *Technical Notes*, Propositions 9.2.2, p. 226, 9.2.3, p. 227 and 9.2.5, p. 229. On the long physical clock the noise amplitude is $g_\delta = \delta^{(1-a)/2}$. Its completed covariance with an original control contains the product $g_\delta \delta^{a/2} = \sqrt{\delta}$. The factor $\delta^{a/2}$ alone is not the physical noise amplitude.

The compact Young perturbation of the free flow has norm at least one on the ambient phase, by *Technical Notes*, Lemma 10.1.1, p. 235. Its real symplectic conservation is a distinct identity. The lower norm bound does not follow merely by treating the weak symplectic form as the phase norm. It makes the logarithmic endpoint functional well defined with the specified truncation at one.

The Gaussian block tuple is realized in its closed separable path span, and its Cameron–Martin map is the original mean map. Closed tube radii and Borel endpoint functionals are proved there. The radial Gaussian bound has a single cost $\|\Phi\|_{H_I}^2/2$. Finite Gaussian regression and compact approximation justify the passage to the full

tuple; neither independent block costs nor a fictitious trace-class time covariance is used. The exact geometry and action statements are *Technical Notes*, Proposition 10.2.1, p. 242, *Technical Notes*, Lemma 10.2.2, p. 244, *Technical Notes*, Proposition 10.2.3, p. 245 and *Technical Notes*, Lemma 10.2.8, p. 250.

8.2 Uniform products and a signed variational expression

On the E phase, the primitive and growth estimates have power $\nu < 2$. The good and bad cell argument retains the final, possibly shorter interval, however short it is. Residuals are controlled first as $\delta \downarrow 0$, then by the residual norm threshold and finally by the coarse block length tending to infinity. The polynomial localization threshold is chosen with exponent $s > r(3 + k_*)/(r - \nu)$, where k_* is the exponent in the polynomial bound $M_B = c_{\mathrm{ball}} B^{k_*}$ with $c_{\mathrm{ball}} > 0$ and $k_* \geq 0$, not the model exponent $k = 3 - \alpha$. The residual denominator is bounded below by one. There is no unproved diagonal choice of radius and approximation. These bounds are the content of Technical Notes, Section 10.3; the primitive and growth statement is *Technical Notes*, Lemma 10.3.4, p. 255.

Define the signed variational expression

$$\mathcal{S}_R = \sup_{\Phi \in H_I} \{2 \operatorname{Rate}_R(\Phi) - \|\Phi\|_{H_I}^2/2\}. \tag{8.1}$$

The completed potential may be signed; positivity is not assumed here. Since $\operatorname{Rate}_R(\Phi) \leq 1 + C_{\mathrm{mean}}\|\Phi\|$, completing the square shows

$$0 \leq \mathcal{S}_R \leq 2 + 2C_{\mathrm{mean}}^2. \tag{8.2}$$

The zero control gives the lower bound, since the free spectral bottom is zero. This ceiling is auxiliary and need not be sharp. The tube and product estimates yield the operator-moment upper bound in *Technical Notes*, Proposition 10.5.4, p. 269.

8.3 Averages of squares, not a rough point trace

The final passage to a point is made with the same source, not by applying a nonexistent point trace on $H^{1/2}$. Put $L_\delta = \delta^{-1}$, $\Gamma_\delta = g_\delta^2 \Gamma$, $D = B_1(0)$ and $\psi_\delta = \eta(\cdot/R_\delta)$. The compact datum $(\psi_\delta, 0)$ equals $(1, 0)$ on the required backward cone. The endpoint P_δ is the physical wave at time L_δ driven by the fast noise constructed from the original Gaussian family, amplitude g_δ and mask m_{R_δ} once. At fixed δ and positive source widths, finite propagation and original stationarity give

$$\mathbb{E}\| \operatorname{pr}_1 P_\delta^{\mathrm{src}}(\psi_\delta, 0)\|_{L^2(D)}^2 = |D|\, \mathbb{E}|u_{\Gamma_\delta, \mathrm{src}}(L_\delta, 0)|^2. \tag{8.3}$$

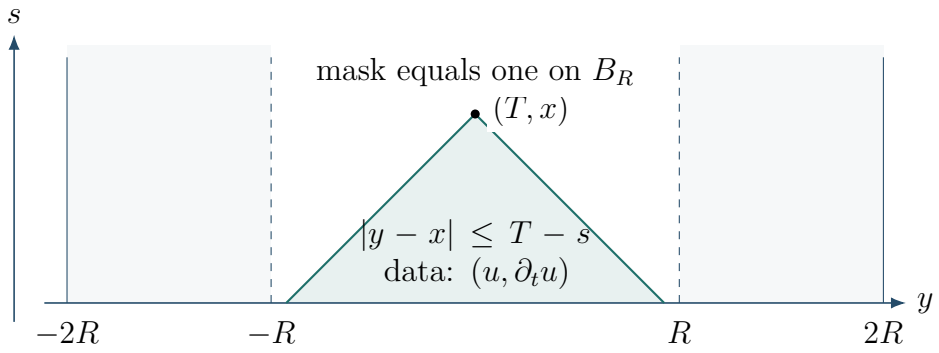


Figure 8: A spatial cross-section of finite propagation. The entire backward cone is chosen inside the region where the mask equals one; the mask vanishes outside $\overline{B}_{2R}$. The drawing is schematic and does not prescribe a value of R/T. Shading indicates the domain of dependence, not a Green density; in dimension three the Green measure is supported on a sphere. In the point-moment comparison, $L = \delta^{-1}$, $R = L + 2$ and $x \in B_1$. Both displacement and velocity must be passed between time intervals. See *Technical Notes*, Lemma 7.2.5, p. 182 and *Technical Notes*, Proposition 10.4.5, p. 264.

It is the integral of expected squares. The square of a spatial average is a different quantity. Source convergence of the E flow transfers the left side; the canonical source moment limit transfers the right side. Only then does exact same-model scaling identify the original time $T_\delta = \delta^{-1/\kappa}$. The compact-data norm contributes a factor whose logarithm multiplied by δ tends to zero. This is *Technical Notes*, Proposition 10.4.5, p. 264. Together with the signed variational expression estimate it gives

$$\limsup_{T\to\infty} T^{-\kappa} \log \mathbb{E}|u_\Gamma(T, x)|^2 \le \limsup_{\delta\downarrow 0} \mathcal{S}_{R_\delta}. \tag{8.4}$$

Both sides are for the same original canonical point solution.

9 Identifying the limiting constant

9.1 Singular Gram matrices are allowed

For vectors k_i in a real Hilbert space, positive weights ℓ_i and nonnegative b_i, let $C_{ij} = \langle k_i, k_j \rangle$. When C has nonnegative entries, consider

$$F_C(\Phi) = 2\sum_i \ell_i \sqrt{(\langle \Phi, k_i \rangle - b_i)_+} - \|\Phi\|^2/2. \tag{9.1}$$

The finite optimization must retain zero vectors and indices with zero contribution. There is no inverse-Gram assumption. For an active subset A of $\{i : C_{ii} > 0\}$ its dual is

$$D_A(w) = \sum_{i\in A} \frac{\ell_i^2}{w_i} - \sum_{i\in A} b_i w_i + \frac{1}{2}\sum_{i,j\in A} w_i C_{ij} w_j, \qquad w_i > 0. \tag{9.2}$$

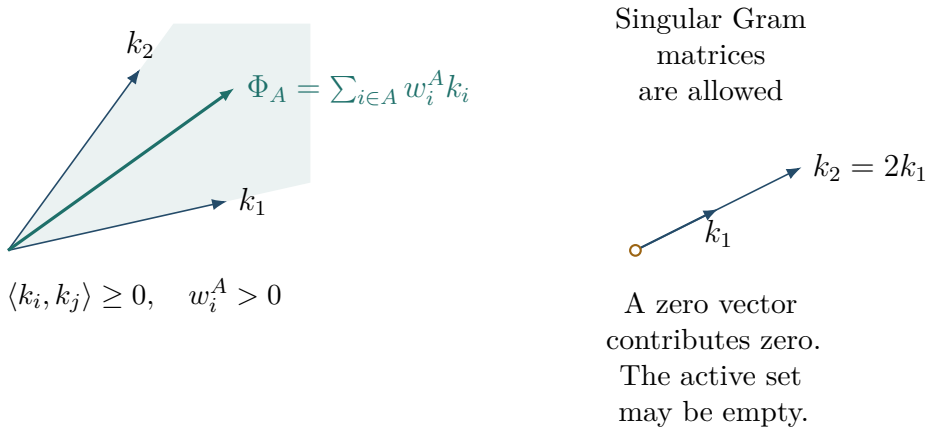


Figure 9: Finite positive combinations, not an inverse covariance formula. For a nonempty maximizing active set, a maximizer has positive coefficients on its selected vectors. The right panel shows why linear independence must not be imposed. The drawing is in a finite-dimensional span and does not restrict the ambient Hilbert space. Neither the maximizing subset nor the maximizer is asserted to be unique. See *Technical Notes*, Proposition 11.1.3, p. 272.

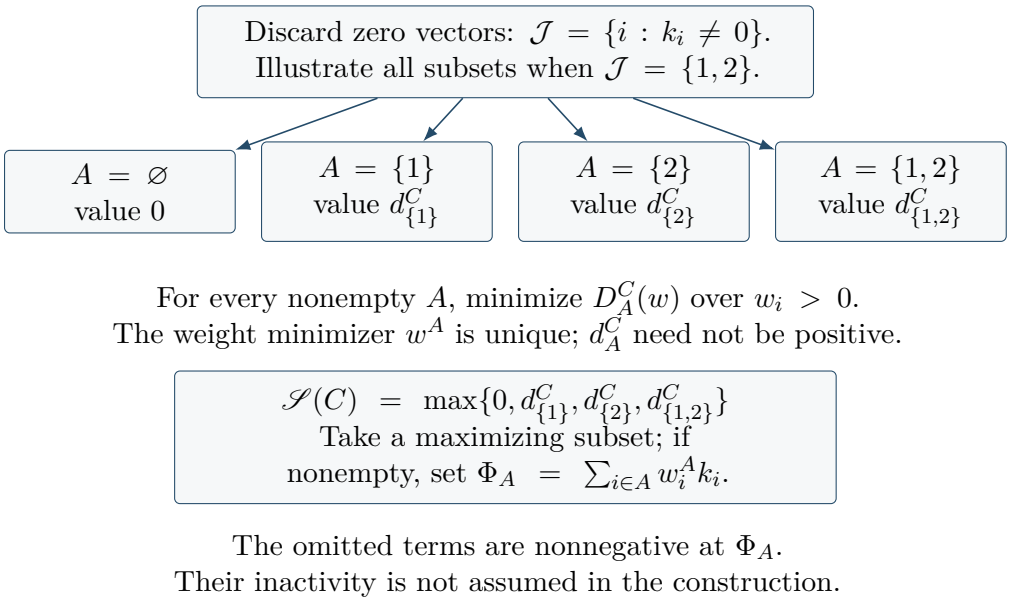


Figure 10: The finite-subset identity includes the empty set with value zero. For each nonempty subset the inner problem is a strictly convex minimization in positive weights, followed by a maximum over subsets. This does not assert global concavity of the original objective, uniqueness of its maximizer, or an effective algorithm. No inverse Gram matrix is used, so coincident vectors and singular Gram matrices remain allowed. See *Technical Notes*, Lemma 11.1.2, p. 271 and *Technical Notes*, Proposition 11.1.3, p. 272.

The active-subset formula includes the empty set, with value zero. The positive conic maximizer and entrywise comparison are *Technical Notes*, Propositions 11.1.3, p. 272 and 11.1.5, p. 274. This is entrywise order for nonnegative Gram entries, not Loewner order on arbitrary covariance operators.

For intuition, the two elementary identities used at an interior active optimum are

$$2\ell\sqrt{x} = \inf_{w>0}\{wx + \ell^2/w\} \quad (x \geq 0), \qquad \sup_{\Phi}\{\langle \Phi, k\rangle - \|\Phi\|^2/2\} = \|k\|^2/2.$$

A zero diagonal forces a zero vector. It cannot create a positive active contribution. The proof treats boundaries before applying these identities and therefore covers singular and zero Gram matrices.

9.2 Bounds for the optimizing controls

Apply this finite optimization to the completed rows of the physical mean. Row normalization is fixed by the original covariance space. The mask appears once. The required optimizer norm is bounded by $M = 4C_{\mathrm{mean}} + 4$, independent of the partition, the trial gradients and R. This is *Technical Notes*, Lemma 11.2.3, p. 277. It is needed *before* the second averaging step: an optimizer chosen after a partition-dependent or gradient-dependent norm threshold would not permit uniform averaging over the same ball. The physical unmasked positive-control vectors dominate the masked Gram entries by *Technical Notes*, Lemma 11.2.2, p. 276. The uniform mean estimates in (7.5) now apply on this one covariance Hilbert ball before family-dependent finite choices. They give

$$\mathcal{S}_R \leq S_2^{\mathrm{pos}} \qquad (R \geq 1). \tag{9.3}$$

This is *Technical Notes*, Proposition 11.2.4, p. 278.

9.3 The cutoff limit and the final deduction

For one fixed $\Psi \in \mathcal{C}_{\mathrm{pos}}$, compactly supported Rayleigh tests see $m_R h_{\Psi,s} \to h_{\Psi,s}$ on their supports. Form comparison and density give convergence of the corresponding rates; their common bound $\sqrt{\sup h_\Psi}$ permits time integration. The variance v_Ψ is unchanged by R. Thus,

$$\liminf_{R\to\infty} \mathcal{S}_R \geq 2I_\Psi - v_\Psi/2.$$

Choose a fixed test arbitrarily close to S_2^{pos} and only then send R to infinity. Together with (9.3) this proves

$$\lim_{R\to\infty} \mathcal{S}_R = S_2^{\mathrm{pos}}. \tag{9.4}$$

No monotonicity of m_R is required. The full proof is *Technical Notes*, Proposition 11.2.5, p. 280.

Proof of Theorem 2.3. Suppose first that $\Gamma \neq 0$. Taking the supremum over fixed tests in (6.2) yields the lower bound S_2^{pos}. Equations (8.4) and (9.4) yield the same upper bound. Both estimates use the same canonical original point solution, exponent κ,

covariance amplitude, initial data and single Gaussian quadratic cost. Hence, the limit exists and equals S_2^{pos}. Proposition 6.1 gives its positivity, finiteness and the factor $2^{q/k}$. If $\Gamma = 0$, all positive-order terms, means and costs vanish; $u = 1$ and both sides are zero. This proves Theorem 2.3. □

10 Calibrations and useful consequences

10.1 Finite orders and comparisons

In one-dimensional spatial white noise with the time-independent calibration, the full order-two coefficient is $t^3/3$ and the full order-four coefficient is $11t^6/540$ in the unit-amplitude convention. Both include self and cross pairings. The order-four calculation has nine representative rows and three representative spatial sectors, giving 27 domain integrals. Restoring the chain-exchanged cases gives five chain splits, three pairings and three sector types, or 45 cases. A row, a sector and a diagram contribution are different levels of that calculation; each level has its own coefficients. The exact tables and finite-domain integrations are *Technical Notes*, Proposition A.1.1, p. 333 and *Technical Notes*, Lemma A.1.2, p. 334. They calibrate the construction and do not identify a full moment constant from finitely many coefficients.

The scalar majorant in the Technical Notes gives order bounds on its logarithmic growth; it is not automatically asymptotic with ratio one. A lower bound on a majorant is not a lower bound on the moment of the solution. The printed spatial three-dimensional constant is optimal in its stated variational calculation; the displayed two-dimensional estimate is a sufficient nonsharp bound.

As $a \downarrow 0$, the exponent in (2.2) tends formally to $(4-\alpha)/(3-\alpha)$, the static scale in [11]. No interchange of the large-time and temporal endpoint limits is asserted by this observation. The separate physical–spectral energy identification in *Technical Notes*, Lemma C.3.1, p. 380 uses [8, Theorem 1.1, p. 2, (1.5)]. It concerns a nonnegative positive-definite homogeneous Radon covariance on $\mathbb{R}^3$ of order $0 < \chi < 2$ and extends the quartic energy to its H^1 domain. The square-root functional in that paper's (1.4) is distinct. This is an auxiliary energy application, not a premise of Theorem 2.2. The static generalized-covariance applications retain their own all-time constants and their asymptotic coefficient types separately. In particular, an all-order enlargement is not an identity for a sharp logarithmic coefficient. The planar singular and endpoint examples remain in Technical Notes, Appendices B and C.

Jensen gives a comparison with the first moment of the solution when its source hypotheses and normalization have been checked. The new variational expression S_1^{pos} is not substituted for that first moment. The Skorohod bounds of [3] are comparisons in their stated scope, not Stratonovich premises.

10.2 Spatial white noise: an energy and bounds, not an exact evaluation

For $d = 1$ and $\Gamma = c\delta_0$, $c \geq 0$, the common spatial energy is

$$\mathcal{E}_{\mathrm{sp}} = \sup_{\substack{f \in H^1(\mathbb{R};\mathbb{R}) \\ \|f\|_2 = 1}} \left\{ c \int_{\mathbb{R}} f^4 - \frac{1}{2} \int_{\mathbb{R}} (f')^2 \right\} = c^2/6.$$

This is *Technical Notes*, Proposition 11.4.2, p. 288. For completeness, the full-profile square identity there gives $3(\int f^4)^2 \leq \int (f')^2$. If $A = \int f^4$, then $cA - \int (f')^2/2 \leq c^2/6 - 3(A - c/3)^2/2$. For $c > 0$, the unit profile $f(x) = \sqrt{c/2}\,\mathrm{sech}(cx)$ has $\int f^4 = c/3$ and $\int (f')^2 = c^2/3$, and attains this energy. It is an H^1 profile, not itself a compact stochastic control. The energy is not $C_2(c, a)$. The occupation comparison and temporal equilibrium give

$$\frac{2}{3}\sqrt{\frac{c}{M_a}} \leq C_2(c, a) \leq \frac{2}{3}\sqrt{cK_0(a)}, \qquad K_0(a) = \frac{2^a}{1-a}, \quad M_a = \frac{\Gamma_E((1+a)/2)}{\Gamma_E(1+a)\Gamma_E((1-a)/2)}. \tag{10.1}$$

Here Γ_E denotes Euler's Gamma function, and the time exponent is $(3 - a)/2$. These are *Technical Notes*, Theorem 11.4.3, p. 289. The occupation ceiling leading to them is in Technical Notes, Section 11.3. It is a derived bound after the intrinsic theorem, not a premise that is used to prove the independent upper estimate. At $c = 0$ both bounds are zero, consistently with $u = 1$.

11 Where the detailed proofs are supplied

The following map gives the shortest reading route through the technical companion. Each item refers to its unchanged statement and full proof there. The companion's *Technical Notes*, Chapter 12, p. 291 explains the failed approaches as numbered results, with proofs and links to the arguments that replace them. For example, *Technical Notes*, No-go 14, p. 311 explains why velocity must be retained across time blocks, and *Technical Notes*, No-go 30, p. 324 explains why pointwise convergence alone does not justify a limit of variational suprema. The companion also has a short list of working words and common misreadings, placed before its List of notation.

Required assertion	**Technical Notes reference**
Original covariance and data	Hypothesis 1.2.1, p. 3
Mixed chains and physical mild solution	Propositions 2.1.1, p. 31 and 2.6.2, p. 52
Positive spatial Wick measures and joint fixed orders	Lemmas 2.5.1, p. 44 and 2.5.2, p. 46
Finite pairing product envelope	Lemma 2.4.1, p. 40
Uniform vertex tail	Lemma 2.6.1, p. 50
Full independent point upper	Theorem 3.3.8, p. 88

Required assertion	Technical Notes reference
Both wave variances	Proposition 4.2.5, p. 108
Compact same-noise path	Proposition 5.1.1, p. 126
Constants and full Young flow	Propositions 6.2.4, p. 157 and 6.2.5, p. 158
Gaussian change of law and point lower bound	Propositions 7.2.2, p. 177 and 7.2.7, p. 186
Unmasked rate, dilation and variational expression finiteness	Proposition 7.3.3, p. 190, Lemma 7.3.5, p. 193, Proposition 7.3.6, p. 193
Smooth spatial ratio and full four-linear extension	Propositions 8.2.4, p. 201 and 8.2.5, p. 202
Fractional products and compact mean	Lemma 8.3.1, p. 207, Proposition 8.3.5, p. 210
Radius-uniform mean and spectral bound	Proposition 9.1.4, p. 221 and 10.3.2, p. 251
Gaussian tubes and the Gaussian quadratic cost	Proposition 10.2.3, p. 245, Lemma 10.2.8, p. 250
Same-source average of squares	Proposition 10.4.5, p. 264
Original point upper by signed variational expressions	Proposition 10.5.4, p. 269
Positive Gram comparison	Proposition 11.1.5, p. 274
Uniform optimizer before averaging	Lemma 11.2.3, p. 277
Every-radius comparison and cutoff limit	Propositions 11.2.4, p. 278 and 11.2.5, p. 280
Final intrinsic point theorem	Theorem 11.2.6, p. 281
White spatial energy and moment bounds	Proposition 11.4.2, p. 288, Theorem 11.4.3, p. 289

Higher even moments and the limits of the present point-moment comparison are discussed in *Technical Notes*, Section 1.9, p. 20. The proposed higher-moment constants remain open extensions of the second-moment result.

References

[1] Raluca M. Balan, *Stratonovich solution for the wave equation*, J. Theoret. Probab. **35** (2022), no. 4, 2643–2689, available at 2105.08802. MR4509081

[2] Raluca M. Balan, Le Chen, and Xia Chen, *Exact asymptotics of the stochastic wave equation with time-independent noise*, Ann. Inst. Henri Poincaré Probab. Stat. **58** (2022), no. 3, 1590–1620. MR4452644

[3] Raluca M. Balan and Daniel Conus, *Intermittency for the wave and heat equations with fractional noise in time*, Ann. Probab. **44** (2016), no. 2, 1488–1534. MR3474476

[4] Raluca M. Balan and Jian Song, *Second order Lyapunov exponents for parabolic and hyperbolic Anderson models*, Bernoulli **25** (2019), no. 4A, 3069–3089. MR4003574

[5] Le Chen and Robert C. Dalang, *Moment bounds and asymptotics for the stochastic wave equation*, Stochastic Process. Appl. **125** (2015), no. 4, 1605–1628. MR3310358

[6] Le Chen and Nicholas Eisenberg, *Interpolating the stochastic heat and wave equations with time-independent noise: solvability and exact asymptotics*, Stoch. Partial Differ. Equ. Anal. Comput. **11** (2023), no. 3, 1203–1253, available at 2108.11473. Published version of arXiv:2108.11473v1. MR4624137

[7] Le Chen, Yuhui Guo, and Jian Song, *Moments and asymptotics for a class of SPDEs with space-time white noise*, Trans. Amer. Math. Soc. **377** (2024), no. 6, 4255–4301. MR4748620

[8] Xia Chen, *Exponential asymptotics for Brownian self-intersection local times under Dalang's condition*, Electron. J. Probab. **28** (2023), Paper No. 119, 17. MR4660700

[9] ———, *Time-dependency in hyperbolic Anderson models: Stratonovich regime*, 2026. Author manuscript, available at https://web.math.utk.edu/~xchen3/aap-chen-2025.pdf (retrieved October 26, 2026). Theorem 1.2 supersedes that of arXiv:2510.01412v1.

[10] Xia Chen, Aurélien Deya, Jian Song, and Samy Tindel, *Solving the hyperbolic Anderson model 1: Skorohod setting*, Ann. Inst. Henri Poincaré Probab. Stat. **61** (2025), no. 3, 1794–1814. MR4947171

[11] Xia Chen and Yaozhong Hu, *Hyperbolic anderson equations with general time-independent gaussian noise: Stratonovich regime*, Ann. Probab. **53** (2025), no. 6, 2144–2195, available at 2403.08603. Published version of arXiv:2403.08603. MR4988274

[12] Michel Crouzeix and César Palencia, *The numerical range as a spectral set*, 2017. Author preprint, arXiv:1702.00668v1; numbering used here refers to this version.

[13] Robert C. Dalang, *Extending the martingale measure stochastic integral with applications to spatially homogeneous s.p.d.e.'s*, Electron. J. Probab. **4** (1999), no. 6, 29. MR1684157

[14] Robert C. Dalang, Carl Mueller, and Roger Tribe, *A Feynman-Kac-type formula for the deterministic and stochastic wave equations and other P.D.E.'s*, Trans. Amer. Math. Soc. **360** (2008), no. 9, 4681–4703. MR2403701

[15] Yaozhong Hu and Xiong Wang, *Matching upper and lower moment bounds for a large class of stochastic PDEs driven by general space-time Gaussian noises*, Stoch. Partial Differ. Equ. Anal. Comput. **12** (2024), no. 1, 1–52. MR4709538

[16] Gerald Teschl, *Mathematical methods in quantum mechanics*, Second, Graduate Studies in Mathematics, vol. 157, American Mathematical Society, Providence, RI, 2014. With applications to Schrödinger operators. MR3243083

[17] John B. Walsh, *An introduction to stochastic partial differential equations*, École d'été de probabilités de Saint-Flour, XIV—1984, 1986, pp. 265–439. MR876085